Journal of Applied Mechanics and Technical Physics, Vol. 50, No. 6, pp. 918–926, 2009

FLOW IN A VISCOUS JET ESCAPING THROUGH A SUPERSONIC NOZZLE INTO A SEMI-INFINITE AMBIENT SPACE

V. N. Vetlutsky,* V. L. Ganimedov, and M. I. Muchnaya

UDC 533.697.4

The problem of an axisymmetric gas flow in a supersonic nozzle and in the jet escaping from the nozzle to a quiescent gas is solved within the framework of Navier–Stokes equations. The calculated pressure distribution is compared with that measured in the jet by a Pitot tube. The influence of the jet pressure ratio, Reynolds number, and half-angle of the supersonic part of the nozzle on nozzle flow and jet flow parameters is studied. It is shown that the distributions of gas-dynamic parameters at the nozzle exit are nonuniform, which affects the jet flow. The flow pattern for an overexpanded jet shows that jet formation begins inside the nozzle because of boundary-layer displacement from the nozzle walls. This result cannot be obtained with the inviscid formulation of the problem.

Key words: *nozzle, viscous jet, boundary-layer separation, Navier–Stokes equations, parallelization.*

1. The problem of propagation of a supersonic jet in a quiescent gas, which has numerous applications, is rather important. The first calculations of such flows by Euler equations date back to the early 1970s [1–3]. Constant values of parameters were set in the initial cross section of the jet. Vasenin and Rychkov [1] and Ivanov and Lanyuk [2] considered overexpanded jets and calculated the Mach disk and the subsonic zone behind it. Rychkov [3] considered the jet flow with solid particles. The major research of jet flows was performed later; it is described in [4, 5] where the results calculated by solving equations with ignored viscosity and with specified parameters in the initial cross section were given. Supersonic jets, however, mainly escape from supersonic nozzles; therefore, the behavior of these jets depends substantially on the nozzle flow.

The jet flow is accompanied by the formation of zones with high gradients of parameters, where viscosity and thermal conductivity play an important role. The results of the first calculations of jet flows by the full Navier–Stokes equations were published in [6, 7], where underexpanded jets with constant flow parameters in the initial cross section were considered.

Mate et al. [8] studied a supersonic jet in experiments and in Navier–Stokes computations. The fields of density and rotational temperature were obtained by means of Raman spectroscopy. Constant values of flow parameters were set in the initial cross section of the jet in the computations, and velocity profiles were defined in the boundary layer. The flow field with a vortex formed behind the Mach disk was obtained in the case of an underexpanded jet. The computed and experimental results are in good qualitative agreement, but the differences in quantitative characteristics are fairly noticeable.

*Deceased.

Khristianovich Institute of Theoretical and Applied Mechanics, Siberian Division, Russian Academy of Sciences, Novosibirsk 630090; ganim@itam.nsc.ru. Translated from Prikladnaya Mekhanika i Tekhnicheskaya Fizika, Vol. 50, No. 6, pp. 6–15, November–December, 2009. Original article submitted November 26, 2007; revision submitted November 27, 2008.

Apparently, the first study of the influence of the nozzle flow on the jet behavior was performed by Tereshenko et al. [9] who calculated first the nozzle flow and then the jet flow by Navier–Stokes equations. The boundary conditions at the jet beginning were taken from the solution of the first problem, but this solution was obtained inside the nozzle, at a certain distance from the nozzle exit, rather than at the nozzle exit proper. Thus, errors of calculating the flow at the nozzle exit, which are caused by artificial boundary conditions, were eliminated.

Kweon et al. [10] studied the influence of a reflector mounted at the nozzle exit on the supersonic jet flow. The reflector size was found to exert a significant effect on the characteristics of overexpanded jets and a minor effect on the characteristics of underexpanded jets.

In the present work, the problem of a viscous flow in a supersonic axisymmetric nozzle and in the jet escaping from this nozzle is solved simultaneously in both domains. In such a formulation, the problem solution was obtained in [11, 12]. Gross and Weiland [11] considered the flows in contoured nozzles of rocket motors and studied flow regimes in detail for various nozzle contours and jet pressure ratios. As the nozzle flow was nonisobaric, oblique shocks and the Mach disk were formed inside the nozzle and a recirculation zone was formed behind the nozzle. Xiao et al. [12] also obtained an off-design flow in a conical nozzle with shock waves and Mach disks and studied the effect of the jet pressure ratio on the flow pattern.

2. We consider the problem of a laminar flow of a viscous gas in a supersonic nozzle and gas exhaustion into an ambient space. The nozzle contour including subsonic, transonic, and supersonic segments is defined by the equation $r = R(x)$ on the segment $0 \leqslant x < X_1$, where the value $x = 0$ corresponds to the nozzle entrance. The supersonic jet escapes into a semi-infinite space filled with a quiescent gas having a specified pressure and temperature. The computational domain for the jet has finite dimensions: its x size is limited by the solid wall $x = X_1$, $r > R_1$ (R_1 is the nozzle radius at the nozzle exit) and by the parallel plane $x = X_2$. In the radial direction, the conditions at infinity are shifted to a cylindrical surface of radius R_2, which is chosen at a sufficiently large distance, so that the boundary conditions on this surface do not affect the process of jet formation. Thus, the problem solution is sought in the domain $\Omega = \{0 \leqslant x \leqslant X_2,\ 0 \leqslant r \leqslant R_b(x)\}$, where

$$R_b(x) = \begin{cases} R(x), & 0 \leqslant x < X_1, \\ R_2, & X_1 \leqslant x \leqslant X_2. \end{cases}$$

The Navier–Stokes equations for the unsteady flow are written in divergent form in the variables $\xi = x/R_*$ and $\eta = r/R_b(x)$ (R_* is the radius of the minimum cross section of the nozzle):

$$\frac{\partial \boldsymbol{U}}{\partial t} + \frac{\partial \boldsymbol{F}_{\text{inv}}}{\partial \xi} + \frac{\partial \boldsymbol{G}_{\text{inv}}}{\partial \eta} + \frac{\partial \boldsymbol{F}_{\text{vis}}}{\partial \xi} + \frac{\partial \boldsymbol{G}_{\text{vis}}}{\partial \eta} + \nu \boldsymbol{S}_{\text{inv}} + \nu \boldsymbol{S}_{\text{vis}} = 0.$$

Here, we have

$$\boldsymbol{U} = J^{-1} \begin{pmatrix} \rho \\ m \\ n \\ e \end{pmatrix}, \qquad \boldsymbol{F}_{\text{inv}} = J^{-1} \begin{pmatrix} \tilde{m} \\ \tilde{m} m/\rho + \xi_x p \\ \tilde{m} n/\rho + \xi_r p \\ \tilde{m}(e+p)/\rho \end{pmatrix},$$

$$\boldsymbol{G}_{\text{inv}} = J^{-1} \begin{pmatrix} \tilde{n} \\ \tilde{n} m/\rho + \eta_x p \\ \tilde{n} n/\rho + \eta_r p \\ \tilde{n}(e+p)/\rho \end{pmatrix}, \qquad \boldsymbol{S}_{\text{inv}} = \frac{J^{-1}}{r} \begin{pmatrix} \tilde{n} \\ \tilde{n} m/\rho \\ \tilde{n} n/\rho \\ \tilde{n}(e+p)/\rho \end{pmatrix},$$

$$\boldsymbol{F}_{\text{vis}} = \frac{J^{-1}}{\text{Re}} \begin{pmatrix} 0 \\ -\tilde{\tau}_{xx} \\ -\tilde{\tau}_{rx} \\ -u\tilde{\tau}_{xx} - v\tilde{\tau}_{rx} + \tilde{q}_x \end{pmatrix}, \qquad \boldsymbol{G}_{\text{vis}} = \frac{J^{-1}}{\text{Re}} \begin{pmatrix} 0 \\ -\tilde{\tau}_{xr} \\ -\tilde{\tau}_{rr} \\ -u\tilde{\tau}_{xr} - v\tilde{\tau}_{rr} + \tilde{q}_r \end{pmatrix},$$

$$\boldsymbol{S}_{\text{vis}} = \frac{J^{-1}}{r\,\text{Re}} \begin{pmatrix} 0 \\ -\tau_{xr} \\ -\tau_{rr} + \tau_{\theta\theta} \\ -u\tau_{xr} - v\tau_{rr} + q_r \end{pmatrix},$$

$$m = \rho u, \quad n = \rho v, \quad \tilde{m} = \xi_x m + \xi_r n, \quad \tilde{n} = \eta_x m + \eta_r n, \quad e = \frac{p}{\gamma - 1} + \frac{m^2 + n^2}{2\rho},$$

$$\tilde{\tau}_{xx} = \xi_x \tau_{xx} + \xi_r \tau_{xr}, \quad \tilde{\tau}_{rx} = \xi_x \tau_{xr} + \xi_r \tau_{rr}, \quad \tilde{\tau}_{xr} = \eta_x \tau_{xx} + \eta_r \tau_{xr}, \quad \tilde{\tau}_{rr} = \eta_x \tau_{xr} + \eta_r \tau_{rr},$$

$$\tilde{q}_x = \xi_x q_x + \xi_r q_r, \qquad \tilde{q}_r = \eta_x q_x + \eta_r q_r,$$

$J^{-1} = \begin{vmatrix} x_\xi & x_\eta \\ r_\xi & r_\eta \end{vmatrix}$ is the Jacobian of coordinate transformation and ξ_x, ξ_r, η_x, and η_r are metric coefficients; the values $\nu = 1$ and $\nu = 0$ refer to the axisymmetric and plane flows. All flow parameters are normalized to the critical velocity of sound a_* and critical density ρ_*, and the pressure is normalized to $\rho_* a_*^2$. The radius of the minimum cross section of the nozzle R_* is used as the linear scale. The friction stress tensor components τ_{xx}, τ_{xr}, and τ_{rr} in the x and r directions, the component $\tau_{\theta\theta}$ in the circumferential direction, and the heat-transfer vector components q_x and q_r have the following form:

$$\tau_{xx} = \mu\Big[\frac{4}{3}\Big(\xi_x \frac{\partial u}{\partial \xi} + \eta_x \frac{\partial u}{\partial \eta}\Big) - \frac{2}{3}\Big(\xi_r \frac{\partial v}{\partial \xi} + \eta_r \frac{\partial v}{\partial \eta}\Big) + \nu \frac{v}{r}\Big],$$

$$\tau_{xr} = \mu\Big(\xi_r \frac{\partial u}{\partial \xi} + \eta_r \frac{\partial u}{\partial \eta} + \xi_x \frac{\partial v}{\partial \xi} + \eta_x \frac{\partial v}{\partial \eta}\Big),$$

$$\tau_{rr} = \mu\Big[\frac{4}{3}\Big(\xi_r \frac{\partial v}{\partial \xi} + \eta_r \frac{\partial v}{\partial \eta}\Big) - \frac{2}{3}\Big(\xi_x \frac{\partial u}{\partial \xi} + \eta_x \frac{\partial u}{\partial \eta}\Big) + \nu \frac{v}{r}\Big],$$

$$\tau_{\theta\theta} = \mu\Big[\frac{4}{3}\nu \frac{v}{r} - \frac{2}{3}\Big(\xi_x \frac{\partial u}{\partial \xi} + \eta_x \frac{\partial u}{\partial \eta} + \xi_r \frac{\partial v}{\partial \xi} + \eta_r \frac{\partial v}{\partial \eta}\Big)\Big],$$

$$q_x = -\frac{\lambda}{(\gamma - 1)\mathrm{Pr}}\Big(\xi_x \frac{\partial T}{\partial \xi} + \eta_x \frac{\partial T}{\partial \eta}\Big), \qquad q_r = -\frac{\lambda}{(\gamma - 1)\mathrm{Pr}}\Big(\xi_r \frac{\partial T}{\partial \xi} + \eta_r \frac{\partial T}{\partial \eta}\Big).$$

The problem is solved under the following boundary conditions. The boundary layer at the nozzle entrance is assumed to be thin; therefore, the values of the entropy function and the Bernoulli constant are unchanged over the entire cross section and equal to the values in the settling chamber S_0 and H_0. In addition, the transverse component of velocity and the derivative of the streamwise component over the coordinate ξ are assumed to have zero values. The streamwise component of velocity cannot be prescribed in advance, because its value depends on the nozzle contour and can be determined only in the course of solving the problem. The no-slip conditions and the condition of an isothermal wall with a constant temperature T_w are set on the nozzle wall and on the vertical solid wall. The conditions of symmetry are imposed on the nozzle and jet axes. The conditions at rest with the gas temperature T_∞ and pressure p_∞ were set on the outer boundary of the ambient space. The "soft" conditions of zero values of the second derivatives of the sought functions were imposed on the right boundary. The thus-formulated boundary conditions are written as follows:

$$\begin{aligned}
&\xi = 0: && \frac{\gamma}{\gamma - 1}\frac{p}{\rho} + \frac{u^2 + v^2}{2} = H_0, \quad \frac{p}{\rho^\gamma} = S_0, \quad \frac{\partial u}{\partial \xi} = 0, \quad v = 0,\\
&\xi = \xi_1,\ r > R_1: && u = 0, \quad v = 0, \quad T = T_w,\\
&\xi = \xi_2: && \frac{\partial^2 f}{\partial \xi^2} = 0, \quad f \equiv u, v, \rho, e,\\
&\eta = 0: && \frac{\partial \rho}{\partial \eta} = 0, \quad \frac{\partial u}{\partial \eta} = 0, \quad v = 0, \quad \frac{\partial e}{\partial \eta} = 0,\\
&\eta = 1,\ \xi \leqslant \xi_1: && u = 0, \quad v = 0, \quad T = T_w,\\
&\eta = 1,\ \xi > \xi_1: && u = 0, \quad v = 0, \quad T = T_\infty, \quad p = p_\infty.
\end{aligned}$$

The values of flow parameters calculated by the one-dimensional theory were set in the nozzle at the initial time. The parameters obtained at the nozzle exit were extended to the entire assumed jet, and ambient parameters were set outside the jet. The problem was solved on a finite-difference grid with constant steps over both

coordinates; derivatives with respect to these coordinates were presented by Harten's total variation diminishing (TVD) scheme [13]. The second derivatives were approximated by central differences. The resultant system of ordinary differential equations with derivatives for each grid node with respect to time was solved by the five-step Runge–Kutta method. The steady solution was found by a time-dependent method.

As the length of the solution domain along the x axis is rather large, the problem was parallelized in this direction and was solved on an mvs1000-128 supercomputer of the Siberian Supercomputer Center (Novosibirsk). Parallelization was performed so that the nozzle exit and the vertical wall coincided with the interface where the data exchange between two processors took place, which made the data exchange substantially simpler. The computational domain was divided between the processors to ensure an identical number of difference-grid nodes treated by each processor. The maximum number of processors used was 20, including 4 processors for nozzle computations.

The number of difference-grid nodes in the streamwise direction for one computation variant was 200 or 400 for each processor, and the difference in the velocity coefficients was smaller than 1%. In the transverse direction, the number of nodes was 200 for the nozzle and 1600 for the ambient space. Reduction of the number of nodes to 100 and 800, respectively, changed the axial velocity coefficient by less than 1%. The number of nodes in the boundary layer on the nozzle wall (including the separation region) was 25 out of 200 for the jet pressure ratio $n = p_a/p_\infty = 1$ (p_a is the pressure at the nozzle exit) and 45 for $n = 0.3$. The majority of computations were performed with 200 nodes in the axial direction and 1600 nodes in the radial direction. For the jet pressure ratio $n = 0.3$, however, the effect of the distance from the axis to the upper boundary on the solution turned out to be more pronounced than for other variants, and the number of nodes in the transverse direction was increased to 3200. The total number of nodes of the difference grid for this computation variant exceeded 3,000,000.

First, we performed inviscid computations [14]. The influence of the boundary conditions at the entrance to the subsonic part of the nozzle was elucidated. For this purpose, the entrance section was extended with a cylindrical tube with identical boundary conditions imposed at the tube entrance. The calculations showed that the velocity profiles at the entrance to the constricting section depend substantially on the tube length. In the cross section with the minimum area, however, the difference in these profiles is smaller than 1% and practically disappears in the supersonic part of the nozzle. Hence, this shift of the boundary conditions exerts practically no effect on the jet flow.

The influence of the apex half-angle of the supersonic part of the nozzle on the distribution of flow parameters at the nozzle exit was also studied in the inviscid approximation. For this purpose, we calculated the flow in the nozzle with apex half-angles $\Theta = 5$–20°, for which the one-dimensional theory predicts the corresponding Mach number at the nozzle exit M = 3. The radial distribution of flow parameters at the nozzle exit was found to be substantially nonuniform. Thus, at $\Theta = 20^\circ$, the Mach number changes by 14%, and the pressure changes by 50%. Therefore, it is not correct to set constant values of parameters in the initial cross section of the jet escaping from a conical nozzle.

3. To test the algorithm, the first computations of a viscous flow were performed for comparisons with experimental data [15] where the jet pressure p_t was measured by a Pitot tube in the radial direction at a distance $x/R_a = 0.53$ from the nozzle exit (Fig. 1). The distance from the axis to the upper boundary in Fig. 1 is normalized to the nozzle-exit radius R_a, and the pressure is normalized to its value in the ambient medium p_∞. Zapryagaev et al. [15] studied the jet escaping from a conical nozzle with the apex half-angle equal to 15°. The nozzle length was chosen to obtain the Mach number at the nozzle exit M = 3 in calculations by the one-dimensional theory. The jet pressure ratio was $n = 0.6$. As the pressure at the nozzle exit in a real flow is not constant over the nozzle radius, the jet pressure ratio was determined on the basis of the pressure value for the nozzle contour used, which was taken from one-dimensional calculations, as it was done in experiments. It follows from Fig. 1 that the difference in numerical and experimental data is within 9%. In some publications, the jet is characterized by the ratio $N = p_0/p_\infty$, where p_0 is the pressure in the settling chamber. In our case, we had $N = 22.3$.

Further computations of the viscous flow in a conical supersonic nozzle and of the jet escaping from the nozzle were performed for several values of the jet pressure ratio. The computations were performed for the apex half-angle of the supersonic part of the nozzle equal to 15 and 20°; the dimensionless temperature of the wall and ambient space was 1.2. The Reynolds numbers based on the critical parameters and on the nozzle-throat diameter were $\mathrm{Re}_* = 10^3$ and 10^5.

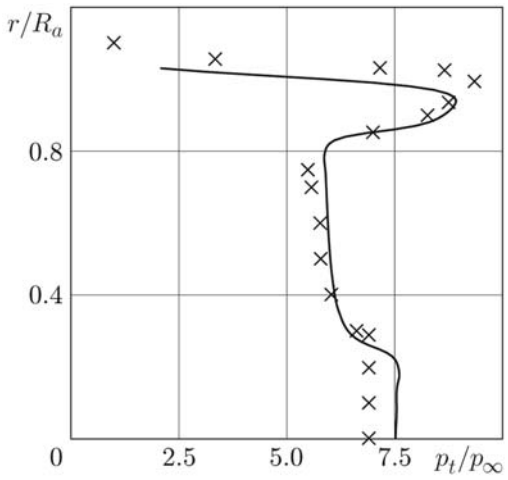

Fig. 1. Pressure in the jet flow obtained in calculations (solid curve) and measured by a Pitot tube [15] (points).

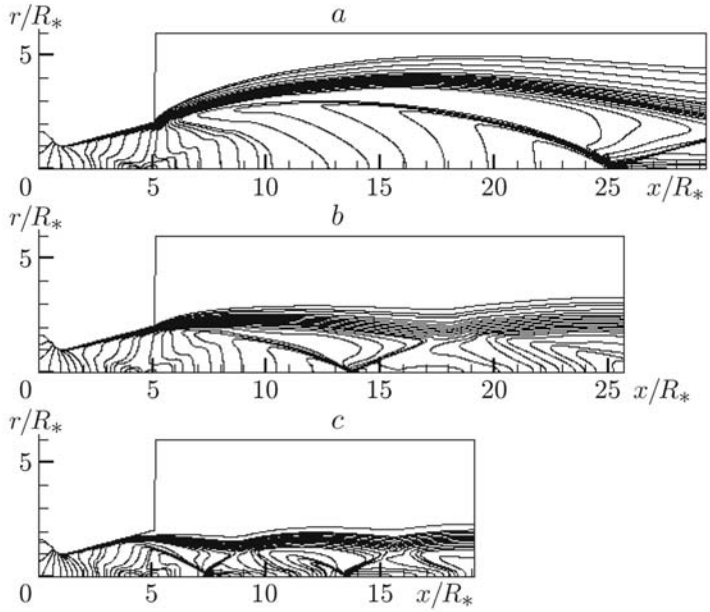

Fig. 2. Mach contours in the nozzle and jet flow for different jet pressure ratios: $n = 3.0$ (a), 1.0 (b), and 0.3 (c).

The results calculated for the apex half-angle of the nozzle $\Theta = 15^\circ$ are summarized in Figs. 2–5. Figure 2 shows the Mach number contours for the jet pressure ratios $n = 3.0$, 1.0, and 0.3, for which $N = 111.50$, 37.15, and 11.15, respectively. In all three variants of the nozzle, an internal shock is formed. This shock is initiated by a discontinuity of curvature at the point of junction of the curved and conical supersonic parts of the nozzle. This shock is reflected from the axis ahead of the nozzle exit and passes to the jet flow. In the first two variants, a barrel shock wave is formed near the nozzle exit, which reaches the jet axis at distances $x/R_* = 25.3$ and 13.6 and becomes reflected from the jet axis to form the Mach disk. The gas is accelerated ahead of the Mach disk to axial Mach numbers M = 6.8 and 4.4, corresponding to $n = 3$ and 1, and then the flow velocity decreases to a subsonic value. The boundary layer grows along the nozzle wall; after a certain time, the boundary layer starts to act as the jet boundary, with high gradients of all parameters. It is in these regions that viscosity and heat conduction play an important role.

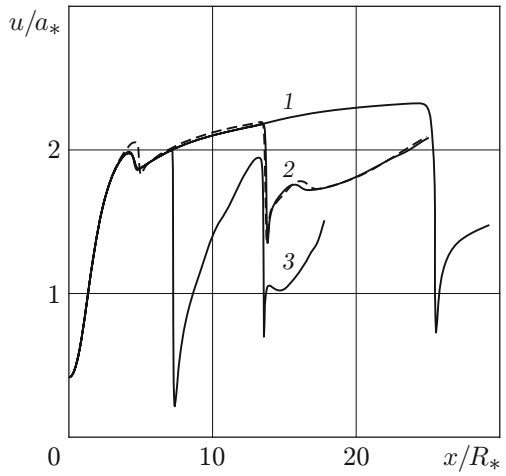

Fig. 3. Axial distribution of velocity for different values of the jet pressure ratio: the solid curves refer to $\mathrm{Re}_* = 10^3$ and $n = 3.0$ (1), 1.0 (2), and 0.3 (3); the dashed curve shows the results for $\mathrm{Re}_* = 10^5$ and $n = 1$.

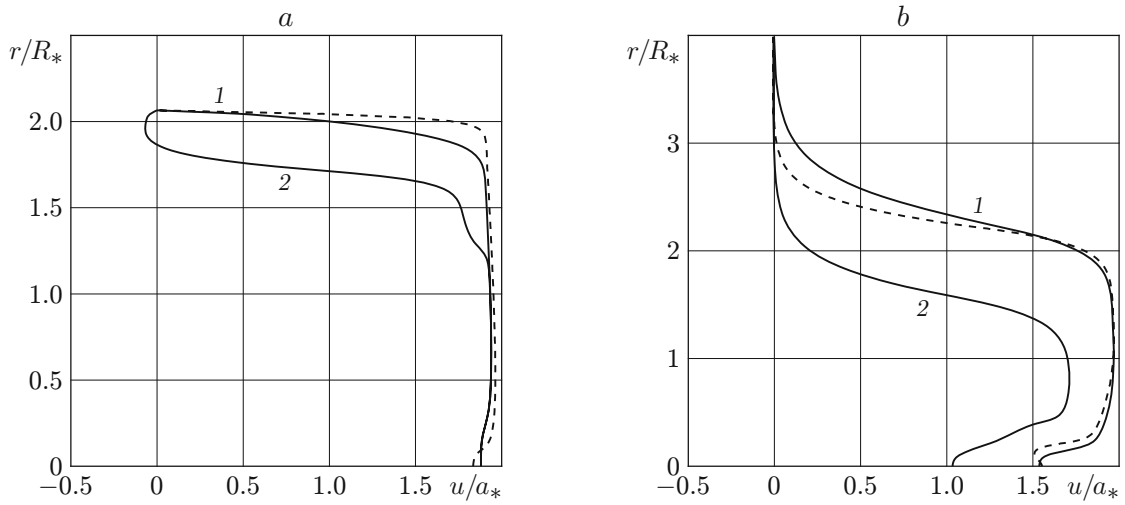

Fig. 4. Velocity profiles at the nozzle exit (a) and in the jet (b): the solid curves refer to $\mathrm{Re}_* = 10^3$ and $n = 1.0$ (1) and 0.3 (2); the dashed curves show the results for $\mathrm{Re}_* = 10^5$ and $n = 1$.

The third variant of calculations differs from the first two variants by the fact that the jet is formed inside the nozzle. Because of the large difference between the pressure at the nozzle exit and the ambient pressure, the gas flows inward the nozzle, thereby displacing the boundary layer from the wall. The boundary layer separates from the nozzle wall at a distance $x/R_* = 3.6$, which shifts the incident shock wave inward the nozzle. The jet boundary is formed at this separation point. After that, the flow is accelerated to the axial Mach number M = 3.2, and then its velocity decreases in the Mach disk located at a distance $x/R_* = 7.2$. Then, the flow is accelerated to the Mach number M = 2.8 and again decelerated at a distance $x/R_* = 13$. It should be noted that such flows cannot be calculated by the Euler equations, because the ambient space affects the nozzle flow via the boundary layer.

The axial distribution of the velocity coefficient u/a_* versus the axial coordinate is plotted in Fig. 3 for three calculation variants mentioned above. The curves $u/a_*(x/R_*)$ clearly show the regions of flow acceleration and deceleration. It is also seen that the gas velocity inside the nozzle at $n = 1$ and $\mathrm{Re}_* = 10^5$ is somewhat higher than that at $\mathrm{Re}_* = 10^3$. The reasons are a thinner boundary layer and a greater core flow in each cross section at a higher Reynolds number. Therefore, the gas in the nozzle flow is accelerated to higher velocities, which alters the jet flow as well.

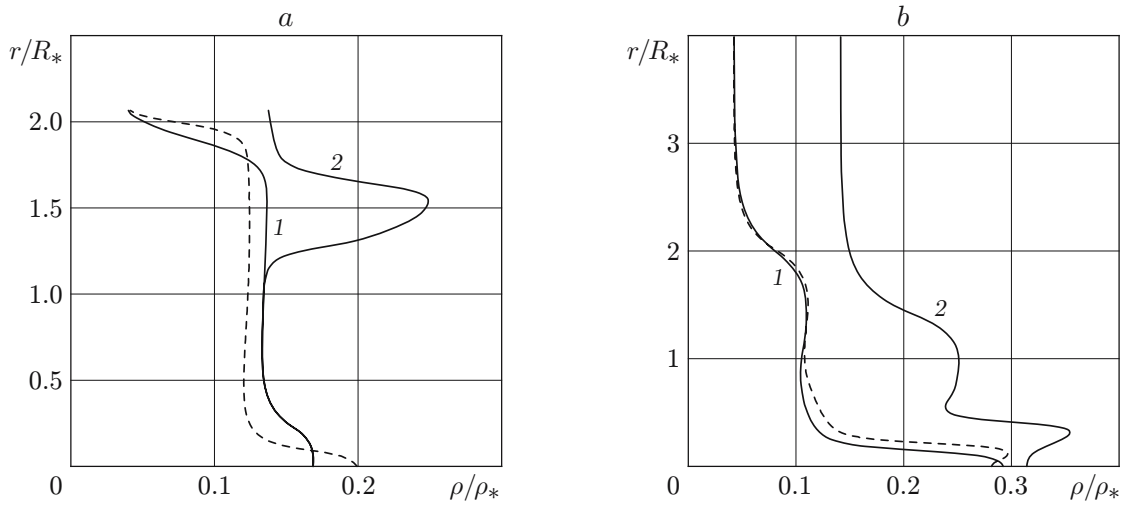

Fig. 5. Velocity profiles at the nozzle exit (a) and in the jet (b) (notation the same as in Fig. 4).

Figure 4a shows the velocity profiles at the nozzle exit at $x/R_* = 5.09$, while the velocity profiles in the jet flow at $x/R_* = 14.0$ are plotted in Fig. 4b. At $n = 1$, the velocity profile at the nozzle exit has a monotonic character. As it could be expected, the boundary layer at $\mathrm{Re}_* = 10^5$ is noticeably thinner than that at $\mathrm{Re}_* = 10^3$. At $n = 0.3$, the near-wall part of the gas enters the nozzle. The shock wave formed at the separation point on the nozzle wall arrives at the point $r/R_* = 1.2$, which is accompanied by an increase in the velocity gradient. The velocity profiles for both jet pressure ratios almost coincide downstream of this point.

The velocity profiles in the cross section $x/R_* = 14.0$ are substantially nonmonotonic. At $n = 1$, the Reynolds number exerts the most pronounced effect near the jet boundary, which becomes more smeared in the case with a greater viscosity. This is also valid for the jet flow with the jet pressure ratio $n = 0.3$. The value of flow velocity near the axis in both calculation variants is considerably lower than that at a certain distance from the axis.

The density profiles at the nozzle exit are monotonic at $n = 1.0$ and nonmonotonic at $n = 0.3$ (Fig. 5a). For the jet pressure ratio $n = 1.0$, the density at the nozzle exit is almost constant over the cross section, except for the boundary-layer region, where the density decreases by more than a factor of 2, and the near-axial region (where the shock formed in the nozzle arrives), where the density increases. The effect of the Reynolds number on the density distribution is manifested in the entire cross section of the nozzle. In the cross section $x/R_* = 14.0$ (Fig. 5b), as well as at the nozzle exit, the density profile is substantially nonmonotonic at $n = 0.3$ and almost monotonic at $n = 1.0$. In the latter case, the Reynolds number exerts a significant effect near the axis.

Figure 6 shows the axial distribution of the velocity coefficient u/a_* at $n = 1.0$, $\mathrm{Re}_* = 10^3$, and two values of the apex half-angle of the conical nozzle: $\Theta = 15^\circ$ (solid curve) and $\Theta = 20^\circ$ (dashed curve). The length of the nozzle with $\Theta = 20^\circ$ was chosen such that the Mach number at the nozzle exit calculated by the one-dimensional theory was equal to 3, as in the case with $\Theta = 15^\circ$. The dimensionless nozzle length was 5.09 in the first variant and 4.24 in the second variant. The abscissa axis is the coordinate x' counted from the nozzle exit. In both calculation variants, the axial velocities at an identical distance from the nozzle exit coincide until the shock wave induced by the discontinuity of curvature at the point of junction of the curved and conical parts of the nozzle arrives on the axis. This happens inside the nozzle in the first case and in the initial part of the jet in the second case. The curves differ substantially in the vicinity of intersection of this shock wave with the axis and in the vicinity of intersection of the shock wave initiated by the nozzle lip with the jet axis, and there is only a minor difference in the other parts of the flow.

4. Thus, an algorithm for calculating a viscous flow in a supersonic nozzle and in the jet escaping from the nozzle into the ambient space was developed. This algorithm is based on the Navier–Stokes equations. The problem is solved with the use of a finite-difference TVD scheme on a multiprocessor computer. The flow field in the nozzle and jet flow is obtained for different values of the jet pressure ratio, Reynolds number, and apex half-angle of the

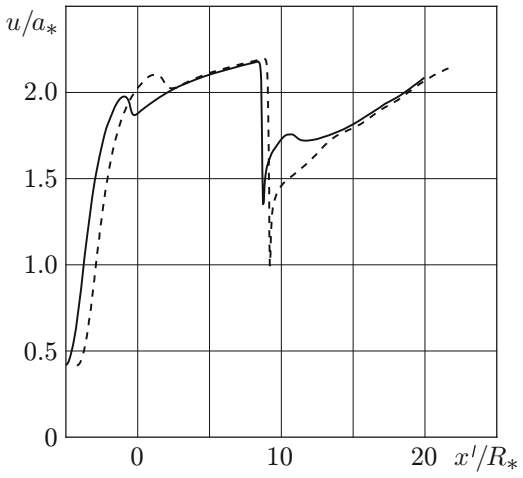

Fig. 6. Velocity distributions at the nozzle and jet axis at $n = 1$: the solid and dashed curves refer to $\Theta = 15$ and 20°, respectively.

supersonic part of the nozzle. The most pronounced effect of viscosity and heat conduction on the flow structure is observed in regions with high gradients: shock waves, boundary layer, and jet boundary. For the jet pressure ratio $n = 0.3$, the inflow of the ambient gas into the nozzle along its wall and the boundary-layer separation are observed, which shifts the incident shock wave inward the nozzle. A change in the apex half-angle of the conical supersonic part of the nozzle leads to significant changes in jet parameters.

REFERENCES

1. I. M. Vasenin and A. D. Rychkov, "Numerical calculation of an axisymmetric supersonic overexpanded jet of an ideal gas," *Izv. Akad. Nauk SSSR, Mekh. Zhidk. Gaza*, No. 5, 197–200 (1970).
2. M. Ya. Ivanov and A. N. Lanyuk, "Calculation of a supersonic overexpanded jet of an ideal gas with the Mach disk present in the flow," *Uch. Zap. TsAGI*, **4**, No. 4, 21–36 (1973).
3. A. D. Rychkov, "Flow of a gas mixture with solid particles in supersonic underexpanded jets," *Izv. Akad. Nauk SSSR, Mekh. Zhidk. Gaza*, No. 2, 75–79 (1974).
4. V. S. Avduevskii, É. A. Ashratov, A. V. Ivanov, and U. G. Pirumov, *Gas Dynamics of Supersonic Nonisobaric Jets* [in Russian], Mashinostroenie, Moscow (1989).
5. V. M. Glaznev, V. I. Zapryagaev, V. N. Uskov, et al., *Jets and Unsteady Flows in Gas Dynamics* [in Russian], Izd. Sib. Otd. Ross. Akad. Nauk, Novosibirsk (2000).
6. L. V. Kuznetsova and B. M. Pavlov, "Calculation of jet flows of a viscous gas," in: *Computational Methods and Programming* (collected scientific papers) [in Russian], Issue 23, Izd. Mosk. Univ., Moscow (1974), pp. 42–53.
7. B. D. Kovalev and V. I. Myshenkov, "Calculation of a supersonic jet escaping into the ambient medium," *Uch. Zap. TsAGI*, **9**, No. 2, 9–18 (1978).
8. B. Mate, I. A. Graur, T. Elizarova, et al., "Experimental and numerical investigation of an axisymmetric supersonic jet," *J. Fluid Mech.*, **426**, 177–197 (2001).
9. A. G. Tereshenko, O. P. Korobeinichev, P. A. Skovorodko, et al., "Probe method for sampling solid-propellant combustion products at temperatures and pressures typical of a rocket combustion chamber," *Combust., Expl., Shock Waves*, **38**, No. 1, 81–91 (2002).
10. Y.-H. Kweon, Y. Miyazato, T. Aoki, et al., "Experimental investigation of nozzle exit reflector effect on supersonic jet," *Shock Waves*, **15**, 229–239 (2006).
11. A. Gross and C. Weiland, "Numerical simulation of separated cold gas nozzle flows," *J. Propuls. Power*, **20**, No. 3, 509–519 (2004).
12. Q. Xiao, H. M. Tsai, and D. Papamoschou, "Numerical investigation of supersonic nozzle flow separation," *AIAA J.*, **45**, No. 3, 532–541 (2007).

13. H. C. Yee, R. F. Warming, and A. Harten, "Implicit total variation diminishing (TVD) schemes for steady-state calculation," *J. Comput. Phys.*, **57**, 327–360 (1985).
14. V. N. Vetlutsky, V. L. Ganimedov, and M. I. Muchnaya, "Influence of the opening angle of a conical supersonic nozzle on the structure of initial interval of non-isobaric jet," *Thermophys. Aeromech.*, **15**, No. 2, 197–204 (2008).
15. V. I. Zapryagaev, A. V. Kudryavtsev, A. V. Lokotko, et al., "An experimental and numerical study of a supersonic jet shock-wave structure," in: *Proc. West East High Speed Flow Fields: Aerospace Applications from High Subsonic to Hypersonic Regime* (Marseilles, April 22–26, 2002), Int. Center for Numer. Methods in Eng., Barcelona (2003), pp. 346–351.